Received: 11 February 2020 | Revised: 22 March 2020 | Accepted: 28 March 2020

DOI: 10.1002/aoc.5729

FULL PAPER

Applied Organometallic Chemistry WILEY

Synthesis, spectroscopic, electrochemical characterization, density functional theory (DFT), time dependent density functional theory (TD-DFT), and antibacterial studies of some Co(II), Ni(II), and Cu(II) chelates of (*E*)-4-(1,5-dimethyl-3-oxo-2-phenyl-2,3-dihydro-1*H*-pyrazol-4-yl)-1-(3-hydroxynaphthalen-2-yl)methylene) thiosemicarbazide Schiff base ligand

Ayman K. El-Sawaf[1,2] | **Yasser K. Abdel-Monem**[2] | **Maged A. Azzam**[1,2]

[1]Department of Chemistry, College of Science and Humanities in Al-Kharj, Prince Sattam Bin Abdulaziz University, Al-Kharj, 11942, Saudi Arabia

[2]Department of Chemistry, Faculty of Science, Menoufia University, Shebin El-Kom, Egypt

Correspondence
Ayman K. El-Sawaf, Department of Chemistry, College of Science and Humanities in Al-Kharj, Prince Sattam Bin Abdulaziz University, Al-Kharj 11942, Saudi Arabia.
Email: elsawaf2008@yahoo.com

Abstract

In this study, mononuclear Co(II), Ni(II), and Cu(II) chelates of the potentially tridentate O, N, S donor ligand (*E*)-4-(1,5-dimethyl-3-oxo-2-phenyl-2,3-dihydro-1*H*-pyrazol-4-yl)-1-(3-hydroxynaphthalen-2-yl)methylene) thiosemicarbazide (H_2L) were synthesized and characterized by elemental analyses, conductivity measurements, Fourier transform infrared spectroscopy, UV–visible spectroscopy, magnetic susceptibility, electron spin resonance (ESR) spectral analysis, thermal thermogravimetric analyses, cyclic voltammetry, and theoretical density functional theory (DFT) and time dependent density functional theory (TD-DFT) studies. The potential donors O (phenolic) and N (azomethine) are found in a *syn* configuration due to a strong intramolecular hydrogen bond [O–H .... N(1)] as shown in the ^1H NMR spectrum of the free ligand. In addition, analytical results revealed the formation of the metal chelates in a ligand-to-metal molar ratio of 1:1. The organic ligand (H_2L) coordinated to the metal center through azomethine nitrogen, phenolate oxygen, and thione/thiolate sulfur groups with the formation of a five- and six-membered rings. The magnetic and spectral results supported the formation of tetrahedral geometry around the Co(II) and Ni(II) centers, while Cu(II) centers were assumed to have a square planar geometry. The time dependent density functional theory (TD-DFT) calculation outputs were used to expect and explain the experimental bathochromic and hypsochromic shifts resulting from the ligand chelation. The antibacterial activity of the compounds under study was evaluated *in vitro* against *Staphylococcus aureus* and *Escherichia coli* demonstrating Gram-positive and Gram-negative bacteria, respectively. It was found that among synthesized compounds, Cu(II) chelate **5** showed the most inhibitory activity against both Gram-positive and Gram-negative bacteria when compared to the organic ligand as well as to the other prepared chelates.

KEYWORDS

antibacterial activity, metal chelates, TD-DFT, thermal studies, Thiosemicarbazone

1 | INTRODUCTION

During the past five decades, there have been much development of research in the coordination chemistry of nitrogen–oxygen–sulfur donor ligands such as substituted thiosemicarbazides, thiosemicarbazones, and dithiocarbazates. Thiosemicarbazones, especially aromatic and heteroaromatic componds, have been used in several applications as depending on the ligand donor atoms, their flexibility and capability to coordinate either in neutral or deprotonated form,[1] they can be used as antitumor agents,[2] anticonvulsants[3] and herbicides.[4] It was found that 2-hydroxy-1-naphthaldehyde thiosemicarbazone and its derivatives can be used as selective agents with cholesterol, glucose, and uric and amino acids in fluorometric determinations, in addition to Fe(II) and Cu(II) in spectrophotometric techniques.[5] Also, a large number of thiosemicarbazone compounds showed medicinal applications owing to their potentially valuable biological properties. Metal chelates that have the capacity to join with nucleobases, DNA fragments, amino acids, peptides, and proteins deserve special attention owing to the clinical use of transition metal chelates as antitumor drugs.[4,6] The biological activities of metal chelates vary from those of either metal ions or ligands and its increased (decreased) as described for many transition metal chelates.[7–9] In continuation of our ongoing interest in the synthesis of new thiosemicarbazone chelates,[10,11] we report here the synthesis, structural characterization, and antibacterial studies of new Co(II), Ni(II), and Cu(II) chelates of (*E*)-4-(1,5-dimethyl-3-oxo-2-phenyl-2,3-dihydro-1*H*-pyrazol-4-yl)-1-(3-hydroxynaphthalen-2-yl)methylene) thiosemicarbazide Schiff base ligand (Scheme 1).

2 | MATERIALS AND METHODS

2.1 | Reagents and instruments

2-hydroxy-1-naphthaldehyde, 4-aminoantipyrine, carbon disulfide, and methyl iodide were obtained from Sigma Aldrich, BDH, and Merck, and used as received. Elemental microanalyses (C, H, and N) were performed by the Microanalytical Unit (Exeter Analytical, Inc. North Chelmsford, MA 01863, USA) within Cairo University (Egypt). Metal elemental analysis and chloride ions were estimated by the usual methods.[12] Infrared spectra were recorded on a Nicolet Fourier transform infrared (FT-IR) spectrophotometer (Thermo Fisher Scientific, North

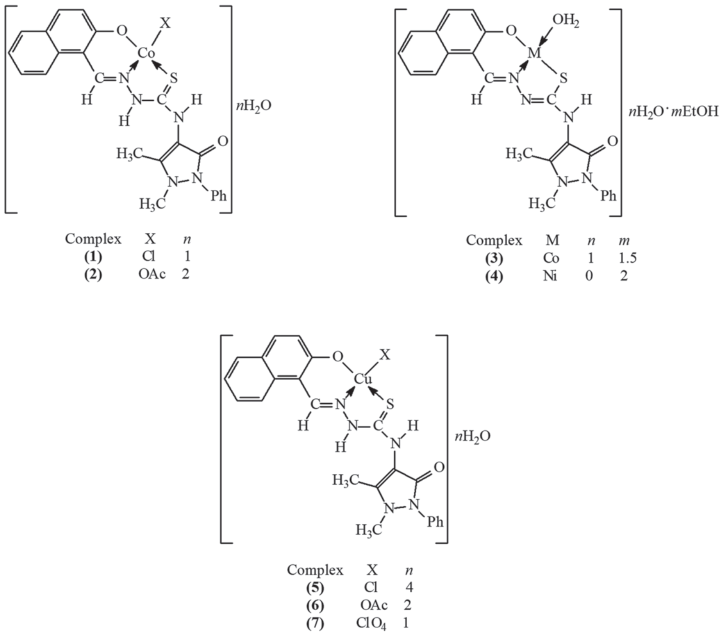

SCHEME 1 Suggested molecular structures of complexes **1**–**7**

Calorina, USA) in the range 4000–400 cm^{-1}. A Varian Cary 5000 spectrophotometer (Varian Inc., Palo Alto, California, USA) was employed to perform the absorption electronic spectra as polycrystalline solid samples. The ^{1}H and ^{13}C NMR spectra of the organic ligand were recorded in deuterated dimethyl sulfoxide (DMSO-d_6) on a Bruker-400 MHz instrument (Bruker Billerica Massachusetts, USA). The fast atom bombardment (FAB) mass spectra were measured using a gas chromatograpy-mass spectrometery (GC-MS, DFS) (Varian Inc., Palo alto, California, USA). The electron paramagnetic resonance (EPR) spectra for polycrystalline samples of Cu(II) chelates were recorded on a Varian E-109c spectrometer (Varian Inc., Palo alto, California, USA) equipped with a field modulation unit at 100 kHz. Measurements were effected in the X-band at room temperature; the microwave power was around 10 mW. Molar conductivity measurements were made in dimethyl formamide (DMF) solution 10^{-3} M using a type CD6N Tacussel conductimeter (Mettler Toledo, Ohio, USA). Thermal gravity-differetial thermal gravity (TG-DTG) analysis was conducted using a Shimadzu DAT/TG-50 thermal analyzer (Shimadzu, Tokyo, Japan) with a heating rate of 10°C/min under a nitrogen atmosphere with a flow rate of 10 drops per minute (dpm) from room temperature up to 1000°C using platinum crucibles. Magnetic susceptibilities were measured at room temperature by a modified Gouy method by using a Johnson Matthey magnetic susceptibility balance (Jhonson Matthey Fabricated Equipment, Wayane Pa. USA). The effective magnetic moments were calculated from the equation $\mu_{eff} = 2.84(X_M{}^{corrt}T)^{1/2}$. Melting points were measured by using Stuart melting point apparatus (Stuart, Cole-Parmer, Staffordshire, UK). Cyclic voltammetry was carried out using a potentiostat (PST 006) from Voltalab-Radiometer Analytical with software model voltaMaster 4 (Hach, SelAgua, Marlboug, Wiltshire, UK). All voltammograms were recorded at 100 mV/s scan rate for the potential range from 2.0 to −0.5 V in DMF containing 0.1 M tetrabutylammonium perchlorate (TBAP) as electrolyte and a three-electrode cell containing a 3 mm GC electrode as a working electrode, a platinum wire as an auxiliary electrode, and silver/silver chloride (Ag/AgCl) as the reference electrode.

2.2 | Synthesis of (*E*)-4-(1,5-dimethyl-3-oxo-2-phenyl-2,3-dihydro-1*H*-pyrazol-4-yl)-1-(3-hydroxynaphthalen-2-yl)methylene) thiosemicarbazide (H_2L)

The organic ligand was synthesized as shown in Scheme 2. 4-(2,3-dimethyl-5-oxo-1-phenyl-2,5-dihydro-1H-pyrazol-4-yl)thiosemicarbazide was synthesized following the previously reported method.[13] (*E*)-4-(1,-5-dimethyl-3-oxo-2-phenyl-2,3-dihydro-1*H*-pyrazol-4-yl)-1-(3-hydroxynaphthalen-2-yl)methylene) thiosemicarbazide (H_2L) ligand was prepared by reacting 4-(2,3-dimethyl-5-oxo-1-phenyl-2,5-dihydro-1*H*-pyrazol-4-yl) thiosemicarbazide (1.65 g, 12.40 mmol) with 2-hydroxy-1-naphthaldehyde (2.00 g, 12.40 mmol) in 70 ml of absolute ethanol. The reaction mixture was kept under reflux at 80°C for 24 hr and monitored by thin-layer chromatography. On completion, the yellow product was filtered off, washed several times with cold ethanol, and air dried under ambient conditions.

2.3 | Synthesis of metal(II) chelates of the Schiff base ligand

Forty milliliters of an ethanolic solution containing 2.72 mmol of the appropriate metal salt was added portionwise to a suspension of the thiosemicarbazone ligand (1.20 g, 2.72 mmol) in ethanol (50 ml) while stirring with gentle warming, and then the reaction mixture was refluxed at 80°C for 10 hr. The resulting color chelates were filtered, washed with anhydrous diethyl ether, and dried in a vacuum desiccator over anhydrous calcium chloride.

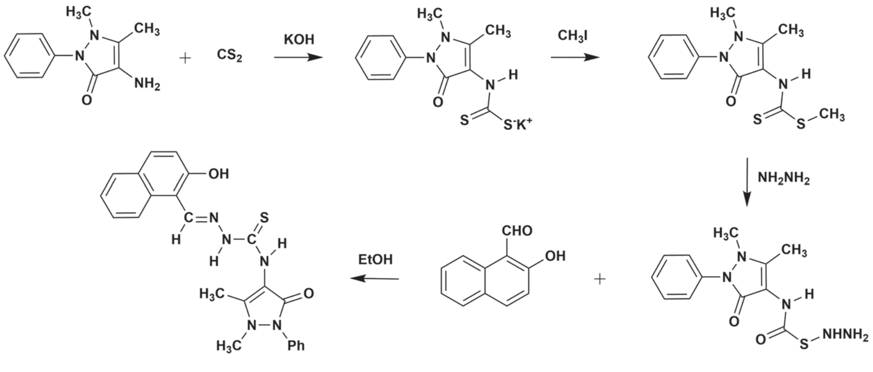

SCHEME 2 Preparation of the organic ligand H_2L

2.4 | Theoretical calculations

Geometry optimization and frequency calculations of the stable conformers of (*E*)-4-(1,5-dimethyl-3-oxo-2-phenyl-2,3-dihydro-1*H*-pyrazol-4-yl)-1-(3-hydroxynaphthalen-2-yl)methylene) thiosemicarbazide (H_2L) were performed using density functional theory (DFT) at the B3LYP/LanL2DZ level of theory.[14] The calculated vibrational modes were scaled by a factor of 0.9679.[15] The maximum electronic absorption bands, vertical electronic excitations, and oscillator strengths ($f > 0$ for allowed transition) of the ligand were calculated using the time dependent density functional theory (TD-DFT) method at the same level of theory.[16,17] NMR magnetic isotropic shielding tensors (σ) were predicted using the gauge-independent atomic orbital (GIAO) approach[18] using the above-mentioned hybrid functionals. The isotropic shielding values were used to calculate the isotropic chemical shifts δ with respect to tetramethylsilane ($Si(CH_3)_4$). $\delta_{\text{iso}}(X) = \sigma_{\text{TMS}}(X) - \sigma_{\text{iso}}(X)$, where δ_{iso} is the isotropic chemical shift and σ_{iso} the isotropic shielding constant. The predicted chemical shifts were obtained using the equation $\delta_{\text{exp}} = a\delta_{\text{cal}} + b$, where $\delta_{\text{cal}} = \delta_{\text{iso}}$. The theoretical calculations in the solvent were obtained using a polarizable continuum model (PCM) in which the solute was embedded into a cavity surrounded by a dielectric continuum solvent described by its dielectric constant (e.g., $\varepsilon CDCl_3 = 4.7113$).[19] The PCM has been reported to correctly model major solvent effects such as the electrostatic effects of the medium providing no specific solute–solvent interactions such as hydrogen bond interactions, dipole–dipole interactions, or induced dipole–dipole interactions are considered.[20] Theoretical calculations were performed using the Gaussian09 package.[21]

2.5 | *In vitro* antibacterial activity

In vitro antibacterial screening of the thiosemicarbazone (H_2L) and its metal chelates was performed at the Department of Parasitology and Animal Diseases, National Research Center, Dokki, Egypt. The bacterial cultures used in this study were *Staphylococcus aureus* as representative for Gram-positive bacteria and *Escherichia coli* as representative for Gram-negative bacteria using the agar diffusion method.[22,23] In all measurements, the concentration of the investigated compounds was 50 mg/ml using dimethyl sulfoxide (DMSO) as solvent control. Dimethyl sulfoxide (DMSO) was used as solvent control and standard enrofloxacin antibiotic discs as used as a positive control in the antibactrial testes. Complete details of the procedure and estimation of the inhibition zones are described elsewhere.[24]

3 | RESULTS AND DISCUSSION

3.1 | Elementary analyses and structural studies

The analytical data and physical properties of the ligand (H_2L) and its metal chelates are shown in Table 1. The results show that the ligand coordinates to the metal ion in a 1:1 molar ratio. Chelates of the monobasic ligand (i.e., loss of phenolic OH proton) are formed with the chlorides of Co(II) and Cu(II), Co(II) acetate, Cu(II) acetate, and Cu(II) perchlorate. Chelates of the dibasic ligand (i.e., loss of OH and N(2)H protons) are formed on chelation with Co(II) nitrate and Ni(II) chloride. All synthesized solid chelates are colored, stable to air and moisture, and soluble in DMF and dimethyl sulfoxide (DMSO). The brown, green, red, and blue colors are common to chelates involving thiosmeicarbazone coordination due to the sulfur to metal charge transfer bands, which dictate their visible spectra.

The molar conductance of the metal chelates was measured in DMF solution (10^{-3} M) and their values (Λ_M) are shown in Table 1. The low molar conductance values of the chelates confirm their nonelectrolytic nature.[25–27] Our effort to grow crystals suitable for X-ray structural determination was unsuccessful.

3.2 | ^{1}H and ^{13}C NMR spectra

One of the most important signs for the formation of H_2L was obtained from the ^{1}H NMR spectrum, where assignments of the signals were established on the chemical shifts and intensity patterns of the ^{1}H NMR spectrum of the thiosemicarbazone ligand (Supporting Information Figure S1 and Table 2). The numbering of the ligand is displayed in its optimized structure obtained at the B3LYP/LanL2DZ level of theory (Figure 1).

The downfield shift of the phenolic OH proton which resonates as singlet signal at δ (ppm) = 11.77 (s, 1H, O–H), in the ligand spectrum indicates the formation of strong intramolecular hydrogen bonding through the N(1) nitrogen atom[28] and confirms that the potential donors O and N(1) are found in a *syn* configuration.[29] Also, the ligand exhibits N(2)H at 10.48 ppm, N(4)H at 9.25 ppm, azomethine proton, N=C(H), at 9.16 ppm, aromatic naphthyl and an *N*-phenyl group of protons as multiplets in the range 8.54–7.22 ppm, N–C(H_3) at

TABLE 1 Colors, partial elemental analyses, and molar conductivities of thiosemicarbazone (H_2L) ligand and its chelates

No	Chemical formula	Formula Weight	Color	Melting point (°C)	Found (calcd %) C	H	N	M	Cl	Λ_M[a]
	$H_2L{\cdot}0.5H_2O$ $C_{23}H_{22}N_5O_{2.5}S$	440.52	Yellow	219	62.52 (62.71)	4.97 (5.03)	16.18 (15.90)	–	–	–
1	[Co (HL)Cl].H_2O $C_{23}H_{22}N_5O_3SCoCl$	542.91	Dark blue	245	50.55 (50.88)	4.05 (4.08)	13.10 (12.96)	10.75 (10.85)	5.94 (5.89)	18
2	[Co (HL)(OAc)].2H_2O $C_{25}H_{27}N_5O_6SCo$	584.52	Yellow blue	238	51.84 (51.37)	4.94 (4.66)	12.75 (11.98)	10.07 (10.08)	–	6
3	[Co(L)(H_2O)].H_2O.1.5EtOH $C_{26}H_{32}N_5O_{5.5}SCo$	593.53	Dark green	240	52.35 (52.62)	5.05 (5.43)	11.71 (11.80)	10.45 (10.85)	–	15
4	[Ni(L)(H_2O)].2EtOH $C_{27}H_{33}N_5O_5SNi$	598.35	Brown red	239	54.37 (54.20)	5.85 (5.56)	11.53 (11.70)	10.25 (10.14)	–	14
5	[Cu (HL)Cl].4H_2O $C_{23}H_{28}N_5O_6SCuCl$	601.58	Dark brown	230	45.73 (45.92)	4.60 (4.69)	11.51 (11.64)	10.83 (10.56)	6.34 (5.89)	20
6	[Cu (HL)(OAc)].2H_2O $C_{25}H_{27}N_5O_6SCu$	589.14	Yellow brown	236	50.76 (50.97)	4.88 (4.62)	11.67 (11.89)	11.51 (10.78)	–	9
7	[Cu (HL)(ClO_4)].H_2O $C_{23}H_{22}N_5O_7SCuCl$	611.53	Dark brown	239	45.07 (45.17)	3.89 (3.63)	11.79 (11.54)	5.35 (5.24)		8

[a] 10^{-3} M in DMF and expressed as Ω^{-1} cm^2 mol^{-1}.

3.13 ppm, and C–CH_3 at 2.52 ppm. The corresponding predicted chemical shifts of the ligand were determined at the B3LYP/LanL2DZ level of theory (Table 2). The correlation curve between the predicted and experimental ^1H NMR chemical shifts is displayed in Figure 2. Relatively good correlation is obtained between the predicted and experimental ^1H NMR chemical shifts with a correlation coefficient of 97.61%.

The structure of the ligand was evaluated further using ^{13}C NMR, where signals for different types of carbon atoms were present in the organic ligand spectrum (Figure S2). The signals observed at 177, 152, and 148 ppm are due to C=S, C=N, and C–O of the thiosemicarbazone moiety, respectively. The spectrum also shows a strong signal at 162 ppm that may be assigned to the C=O of the pyrazolone ring.

3.3 | Mass spectra

The formation and purities of the Schiff base ligand (H_2L) and its metal chelates were confirmed using mass spectrometry. The mass spectrum of the Schiff base ligand H_2L had a molecular ion peak at m/z = 442.5, which agrees with the molecular weight (M + 2). The intensity of the peaks due to fragmentation is shown in Supporting Information Figure S3. Similarly, the mass spectra of metal complexes **1–7** are shown in Supporting Information Figure S4, where the molecular ion peaks can be seen at m/z = 544, 582, 595, 597.3, 603, 592, and 609, respectively. The results obtained from the elemental analyses and mass spectra of the synthesized Schiff base ligand and its metal chelates are consistent with each other, which confirms the proposed molecular formula (Table 1). In addition, the spectra of the compounds showed some additional peaks owing to molecular cations of various fragments of the metal chelates.

3.4 | Infrared spectra

The prominent assignments for the IR spectral bands for the organic thiosemicarbazone ligand and its metal chelates are shown in Table 3. In principle, the organic ligand should display thione–thiol tautomerism, –N(H)–C(=S)– ↔ N=C(–SH)–, since it contains a thioamide –NH–C=S functional group. The absence of any ν(S–H) band, which usually appears in the 2600–2800 cm^{-1} region of the IR spectrum of the ligand (Supporting Information Figure S5), suggests the thionic nature of the organic ligand in the solid state.[30,31]

TABLE 2 Calculated and experimental ^{1}H chemical shifts (ppm) of (*E*)-4-(1,5-dimethyl-3-oxo-2-phenyl-2,3-dihydro-1*H*-pyrazol-4-yl)-1-(3-hydroxynaphthalen-2-yl)methylene) thiosemi-carbazide(H_2L) in deuterated dimethyl sulfoxide (DMSO-d^6)

	Predicted	Experimental
^{1}H NMR		
H1	7.73	7.90
H2	7.55	7.56
H3	7.72	7.93
H6	7.88	8.35
H9	7.47	7.34
H10	7.80	7.93
H11	8.58	9.17
H23	2.59	2.52
H24	3.61	3.13
H26, H30	7.58	7.87
H27, H29	7.67	7.53
H28	7.65	7.24
H13 (NH)	7.79	10.44
H16 (NH)	5.80	9.26
OH	12.40	11.77

The spectrum of the free ligand showed a broad medium band at 3430 cm^{-1} assignable to intramolecular hydrogen bonding between phenolic O–H and the N(1) nitrogen atom.[32,33] The absence of this band in the spectra of all metal chelates provides strong evidence for coordination through the deprotonated phenolic oxygen and this causes ν(C–O) to be blue-shifted by 30–80 cm^{-1} from its position at 1242 cm^{-1} in the ligand spectrum.[34,35] This is also supported by the presence of a new band around 550 cm^{-1} in the spectra of the chelates assignable to ν(M–O).[36] The spectrum of the ligand shows a medium band at 3175 cm^{-1} attributable to ν(N–H).[37] However, this band disappears in the spectra of $[Co(L)(H_2O)].H_2O.1.5EtOH$ and $[Ni(L)(H_2O)].2EtOH$ chelates (Supporting Information Figure S5) due to the change in the tautomerism and subsequent deprotonation of the =N–NH– group. Consequently, a new band due to ν(N=C) is seen at ca. 1580 cm^{-1}.

Other bands were observed at 3040 and 2930 cm^{-1}, and these can be attributed to υ(C–H) of the aromatic and aliphatic vibrations, respectively.[38] A small decrease in the energy (about 5–20 cm^{-1}) of the ν(C=N) band is indicative of coordination via the azomethine nitrogen ion.[39,40] This is further confirmed by the appearance of a new band in the range 480–430 cm^{-1}assignable to ν(M–N).[41] The medium intensity band found at 1150 cm^{-1} owing to ν(N–N) of the thiosemicarbazone was shifted to a higher frequency in the spectra of all chelates, indicating the increase in bond strength, and again endorses coordination via the azomethine nitrogen. A medium intensity band at 865 cm^{-1} corresponding to ν(C=S) in the spectrum of the ligand completely disappeared in the spectra of chelates

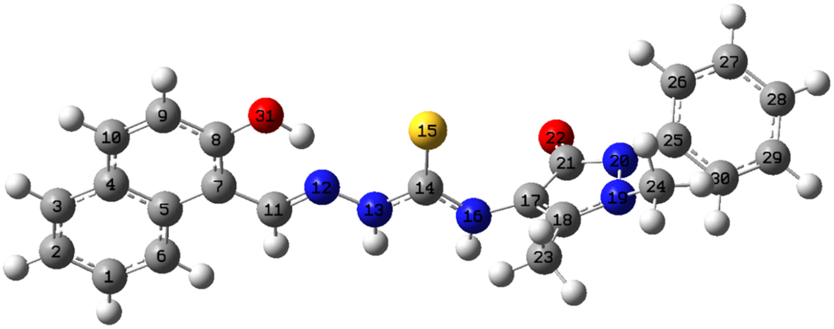

FIGURE 1 The optimized structure of ligand (H_2L) obtained at the B3LYP/LanL2DZ level of theory

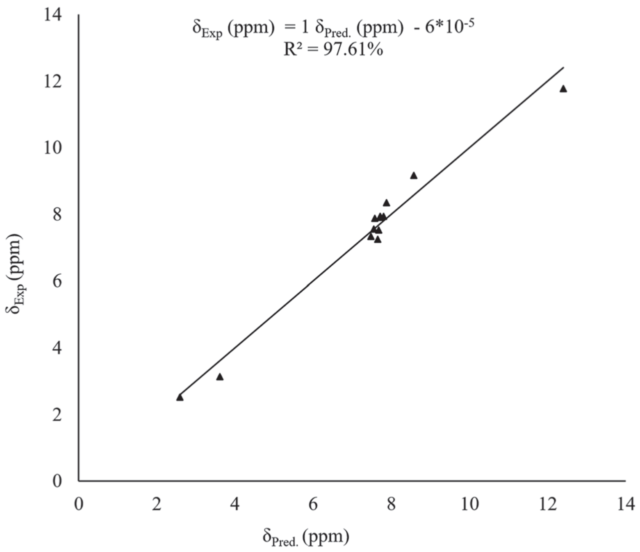

FIGURE 2 Correlation curve between predicted and experimental ^{1}H NMR chemical shifts of the ligand

[Co(L)(H_2O)].H_2O.1.5EtOH (**3**) and [Ni(L)(H_2O)].2EtOH (**4**) (Supporting Information Figure S5), and new bands at 745 and 755 cm^{-1} owing to υ(C–S) indicated the participation of te thiolate sulfur atom through enolization and subsequent deprotonation.[42,43]

The spectrum of the acetato chelate, [Cu (HL)(OAc)].2H_2O, showed two bands at 1625 and 1425 cm^{-1} due to ν_{as}(COO^-) and ν_{sy}(COO^-), respectively, while the corresponding bending modes were seen at 670 and 630 cm^{-1}. The large separation $\Delta\nu = \nu_{as} - \nu_{sy} = 200$ cm^{-1} is indicative for the monodentate geometry of the acetate ligand bonded to Cu (II).[44] The occurrence of coordinated water in chelates **3** and **4** was confirmed by the presence of bands at ca. 3460, 1570, 955, and 655 cm^{-1} due to ν(OH), δ(H_2O), ρ_{rock}(H_2O), and ρ_{wagg}(H_2O), respectively.[45] The last two modes were absent from the spectra of the other chelates with water molecules, indicating hydrated rather than coordinated water.[46]

The spectrum of perchlorate chelate (**7**) showed split strong bands (ν_3) at 1117 and 1049 cm^{-1}, and a strong band at 620 cm^{-1} (ν_4) (Supporting Information Figure S5) in agreement with monodentate coordination of perchlorate.[47] Thus, it may be established that the ligand behaves as a monobasic[48] or dibasic[49] tridentate ONS chelating agent coordinating via azomethine nitrogen, phenolic oxygen, and thione/thiol sulfur.

TABLE 3 Important IR spectral bands (cm^{-1}) of the ligand (H_2L) and its metal chelates

No.	Ligand/chelate	ν[N(2)H]	ν(C=N)	ν(C–O) phenolic	ν(N–N)	ν(C=S)	ν(C–S)	ν(M–O)	ν(M–N)	ν(M–S)
	H_2L·0.5H_2O	3175(m)	1600(s)	1250(s)	960(m)	865(m)	–	–	–	–
1	[Co (HL)Cl].H_2O	3180(w)	1595(s)	1185(m)	985(w)	850(m)	–	575(w)	490(w)	425(w)
2	[Co (HL)(OAc)].2H_2O	3100(m)	1597(m)	1190(m)	1020(m)	825(w)	–	540(m)	460(w)	415(m)
3	[Co(L)(H_2O)].H_2O.1.5EtOH	–	1605(s)	1180(m)	990(s)	–	745(m)	435(w)	450(w)	418(m)
4	[Ni(L)(H_2O)].2EtOH	–	1600(w)	1180(m)	995(s)	–	755(s)	560(m)	465(s)	425(w)
5	[Cu (HL)Cl].4H_2O	3150(m)	1585(s)	1210(m)	1025(s)	815(m)	–	535 (m)	440(m)	422(w)
6	[Cu (HL)(OAc)].2H_2O	3120(w)	1590(m)	1195(m)	1020(w)	835(w)	–	548(w)	460(w)	418(w)
7	[Cu (HL)(ClO_4)].H_2O	3110(w)	1605(s)	1190(m)	995(s)	840(m)	–	550(w)	463(w)	426(w)

TABLE 4 Some of the calculated and predicted vibration modes of the ligand (H_2L) and its [Ni(L)(H_2O)].2EtOH (4) and [Cu (HL)Cl].4H_2O (5) chelates

	H_2L			4			5		
	Cal	Scal	Exp	Cal	Scal	Exp	Cal	Scal	Exp
$\nu_{N\text{-}H}$	3512	3399	3175	3582	3467	–	3537	3423	3150
$\nu_{C=N}$	1610	1558	1600	1610	1558	1600	1615	1563	1585
$\nu_{C\text{-}O}$	1251	1211	1250	–	–	1180	–	0	1210
$\nu_{N\text{-}N}$	1151	1114	960	–	–	995	–	0	1025

Note. Cal, Calculated; Exp, Experimental; Scal, Scaled.

TABLE 5 Magnetic moment and solid state electronic spectral data (nm) of the ligand and its metal chelates

Compound	$\pi \rightarrow \pi^*$	$n \rightarrow \pi^*$	LMCT	d → d	μ_{eff}(B.M.)
H_2L	220 245	280 350	–	–	–
[Co (HL)Cl]· H_2O	260	300 343	395 440	470 640	4.42
[Co (HL)(OAc)]· $2H_2O$	275	315 350	370 450	485 660	4.26
[Co(L)(H_2O)].H_2O.1½EtOH	280	305 335	390 430	430 615	4.35
[Ni(L)(H_2O)].2EtOH	245	305 355	390 445	470 660	2.61
[Cu (HL)(Cl]·$4H_2O$	275	305 350	395 455	465 620	1.75
[Cu (HL)(OAc)] ·$2H_2O$	275	310 380	395 455	480 645	1.89
[Cu (HL)(ClO_4]· H_2O	270	315 355	390 450	460 610	1.81

Note. B.M., Bohrmagneton; LMCT, Ligand metal charge transfer.

Some of the calculated and predicted vibration modes of the ligand and its Ni(II) and Cu(II) chelates are displayed in Table 4. The calculated values are obtained at the B3LYP level of theory and the predicted values are obtained from the calculated and scaled by a factor of 0.9679. As shown in Table 4, ν(C=N) is relatively well predicted with deviations of 42, 42, and 22 cm^{-1} with respect to the experimental values of the ligand, and its metal chelates **4** and **5**, respectively.

3.5 | Magnetic moments and electronic spectra

The magnetic moments values of the metal chelates at room temperature in accordance with the electronic spectral data of the free ligand (H_2L) and its metal chelates are listed in Table 5. The spectra of the organic ligand (H_2L) and its metal chelates were measured in Nujol mull over the range of 200–1000 nm.

The spectrum of the free thiosemicarbazone (Supporting Information Figure S6) shows four absorption bands at 220, 245, 280, and 350 nm. The first two bands are assigned to the intraligand $\pi \rightarrow \pi^*$ transitions while the third band at 280 nm is assigned to $n \rightarrow \pi^*$ charge transfer transition associated with the azomethine and thioamide functional groups overlapping in the same envelope.[50] The $n \rightarrow \pi^*$ transitions at 350 nm are assignable to the phenol (OH) function.[51] The maximum absorption band at 350 nm is overestimated at the B3LYP level of theory in gas and PCM solvent with a variation of 26 nm with respect to the experimental value. This band corresponds to the HOMO → LUMO electronic transition (Figure 3).

The absorption bands at 245 nm are attributed to electronic transitions HOMO-7 → LUMO (37%) and HOMO → LUMO+4. This band is overestimated by 14 nm with respect to the experimental value. These transitions are also found in the spectra of the metal chelates, but they are shifted towards lower and higher frequencies, confirming coordination of the ligand by the metal ions.[52] Based on previous studies of the metal chelates of thiosemicarbazones,[53,54] we assigned a $\pi \rightarrow \pi^*$ band at ca. 270 nm and an $n \rightarrow \pi^*$ band at ca. 300 nm (Table 5). The shift of the $n \rightarrow \pi^*$ bands to longer wavelength region in metal chelates is strong evidence for the coordination of azomethine nitrogen and thioamide sulfur with metal ions.[55] To emphasize the chelation effect on the absorption bands observed in the ligand spectrum, the predicted spectra of the metal chelates **2**, **4**, and **5** were obtained at the B3LYP level of theory (Figure 4). As can be seen in Figure 4, the chelation of the ligand with metal ions induces a bathochromic shift of $\pi \rightarrow \pi^*$. The observed bands at 249 and 276 nm were shifted to 345 and 396 nm, respectively. From the predicted spectra of the ligand and its Ni chelate **4**, it is clear that the

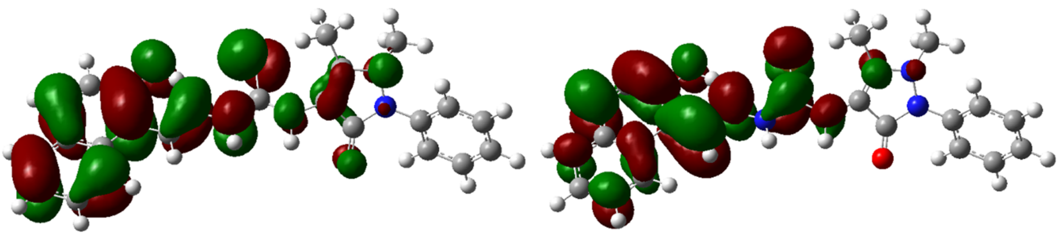

FIGURE 3 HOMO (left) and LUMO (right) frontier orbitals of the ligand H_2L

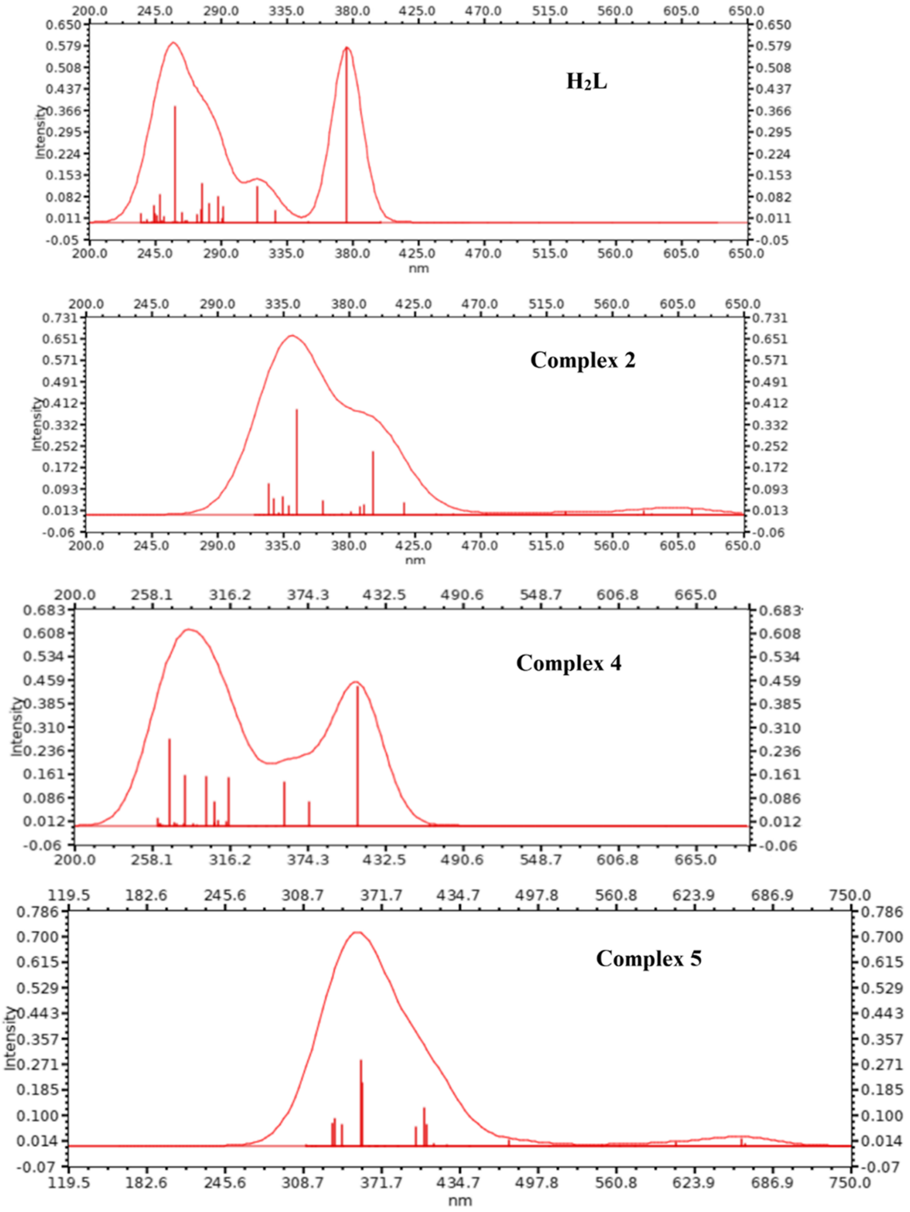

FIGURE 4 Predicted spectra of the ligand H_2L and its complexes **2**, **4**, and **5**

chelation leads to a bathochromic redshift of n → π*. Similarly, the Cu chelate **5** with the ligand leads to a bathochromic shift of π → π*. The HOMO and LUMO orbitals are shown in Figure 5. The HOMO and LUMO orbitals of the **2**, **4**, and **5** metal chelates are displayed in Figure 4. As can be seen from Figure 5, the HOMO → LUMO transition induces a transfer of charge from one side to another in these chelates. For instance, in **4**, the HOMO → LUMO transition induces a transfer of charge from the naphthalene moiety to Cu and its vicinal moieties (Figure 5).

The metal to ligand charge transfer bands are found at 350–400 and 400–450 nm.[56] The lower wavelength band is assigned to S → M(II) transitions, which are quite common in the electronic spectra of metal chelates of thiosemicarbazones,[57] and the higher wavelength band is associated with N → M(II) transitions. It has been shown that the phenolate compounds show a broadening line with a tail running across the visible part of the spectrum resulting from phenolate to metal charge transfer that overlaps on the high wavelength side of S → M(II) transitions. For the metal chelates under study, the O → M(II) transitions are found in the range 290–350 nm.[58]

The electronic spectra of the dark green and blue Co(II) compounds show two bands at ca. 666 and 465 nm which are assigned to $^4A_{2g} \rightarrow {}^4T_{1g}(F)$ (υ_2) and $^4A_{2g} \rightarrow {}^4T_{1g}(P)$ (υ_3) transitions, respectively, revealing typical tetrahedral coordination around the Co(II) ion.[59] The values of ligand field parameters B (interelectronic repulsion of the d electrons in chelate), β (the nephelauxetic effect), and 10Dq are calculated as stated

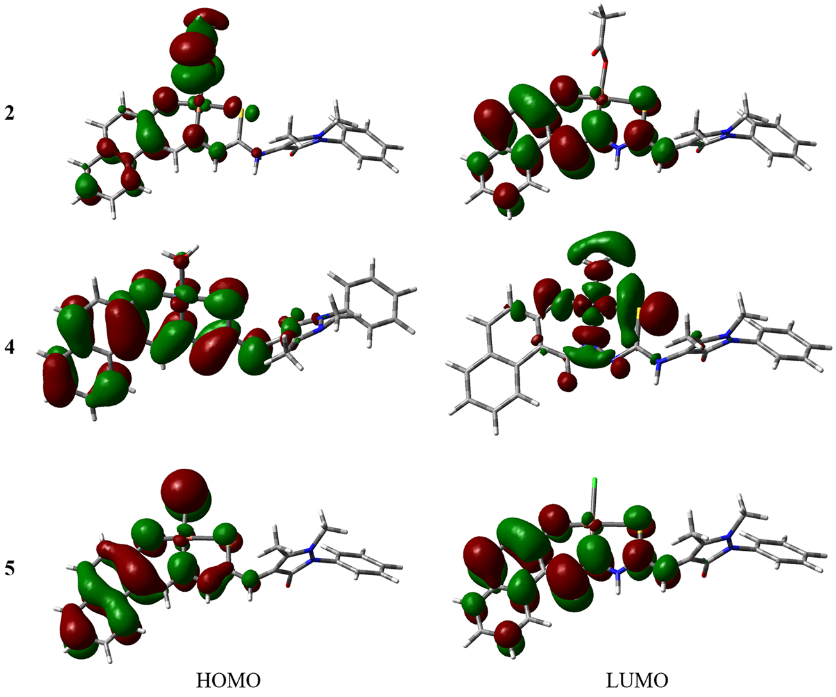

FIGURE 5 HOMO (left) and LUMO (right) frontier orbitals of metal complexes **2**, **4**, and **5**

by the equations reported for the tetrahedral compounds **1**, **2**, and **3**, and their values are found to be in the ranges reported for other tetrahedral Co(II) chelates with sulfur donor atoms.[60,61]

$$\mu_{\mathrm{eff}} = 3.87(1 - 4\lambda/10\mathrm{Dq}), \lambda = -178\,\mathrm{cm}^{-1}$$

$$\mathrm{B} = \left[4(\nu_3 - 15\mathrm{Dq})^2 - 10\mathrm{Dq}^2\right] / [60(\nu_3 - 15\mathrm{Dq}) - 180\mathrm{Dq}]$$

$$\nu_1 = 10\mathrm{Dq}$$

$$\mathrm{B} = \mathrm{B(chelate)}/\mathrm{B(free\,ion)}$$

where B(free ion) for Co(II) is 963 cm^{-1}.

The 10Dq values obtained for metal chelates **1–3** via this method are −5170, −5140, and −4980 cm^{-1}, respectively. These results indicate that the interelectronic repulsion of the d electrons in metal chelates is less than in the free ion. The **B** values for the compounds are about 70% of the free ion value. The reduction of **B** by chelate formation is affected by the delocalization of the d electron cloud on the organic thiosemicarbazone, which is sequentially caused by the formation of the covalent bond.[62] According to Jorgenson, the organic ligand which coordinates via a sulfur donor atom shows a low value of **B** and causes a pronounced nephelauxetic effect.[63] The lower the value of the nephelauxetic effect, β, the greater the extent of covalence. For Co(II) chelates, β values are lower than 1, which provides the information on the covalent nature of the metal–ligand bond. The μ_{eff} values 4.42, 4.26, and 4.35 B.M. for Co(II) chelates **1**, **2**, and **3**, respectively, correspond to three unpaired electrons in a tetrahedral environment.[64] The electronic spectrum of the Ni(II) chelate **4** shows two d–d bands at 470 and 660 nm, the position of the bands indicative of tetrahedral stereochemistry, assigned to $^3T_1(F) \rightarrow {}^3T_2$ (υ_2) and $^3T_1(F) \rightarrow {}^3T_2$ (υ_3) transitions, respectively. More intense bands in the d–d electronic spectrum and high magnetic moment value, $\mu_{\mathrm{eff}} = 2.61$ B.M., support a tetrahedral configuration for the Ni(II) chelate.[65] Cu(II) chelates in the present study show μ_{eff} values of 1.75, 1.89, and 1.81 B.M. for chelates **5**, **6**, and **7**, respectively, corresponding to one unpaired electron. The absorption spectra of Cu(II) chelates are consistent with the earlier report of square planer chelates[46] and show a low intense d–d band in the range 600–650 nm corresponding to $^2B_{1g} \rightarrow {}^2E_g(d_{x^2-y^2} \rightarrow (d_{xz,yz})$, $_2B_{1g} \rightarrow {}^2B_{2g}$ $(d_{x^2-y^2} \rightarrow d_{xy})$, and $^2B_{1g} \rightarrow {}^2A_{1g}$ $(d_{x^2-y^2} \rightarrow d_{z^2})$. Since these lower orbitals are often close in energy, it is difficult to resolve the individual transitions from the lower to upper d level and a single absorption band was observed.[66]

3.6 | Thermal studies

The thermal pyrolysis behavior of the free thiosemcarbazone ligand and its metal chelates were examined by thermogravimetric analysis (TG) and differential thermogravimetry (DTG) in the temperature range of room temperature up to 1000 °C, under an inert atmosphere. The percentage of weight losses found (calcd), temperature range, and interpretation of each pyrolytic step are presented in Table 6 and thermograms are shown in Supporting Information Figure S7. Because of the explosive nature of perchlorate salts, the thermal properties of chelate **7** were not determined.

The thermoanalytical data in Table 6 show that the organic ligand (H_2L) exhibited a weight loss of 2.34% within the range 25–215°C equivalent to a loss of 0.5 mol of water. The ligand undergoes thermal pyrolysis via two degradation steps. The first occurs at 215–390°C and is characterized by a weight loss of 32.03%. This weight is consistent with the elimination of the $C_{10}H_7O$ portion via cleavage of the longest C(7)–C(11) bond in the thiocarbohydrazide backbone. The second weight loss of 59.91% appeared in the range 395–1000°C compatible with the liberation of the $C_{11}H_{14}N_5OS$ fragment. This step is associated with a sharp and broad DTG peak at T_{max} = 485 and 610°C, respectively. The weight percentage of 5.72 (calcd 5.45%) of the final residue indicates that the product of the thermal degradation processes of the thiosemcarbazone ligand is 2 moles of carbon.

The thermal pyrolysis data (Table 6) of the tetracoordinated chelates [Co (HL)Cl].H_2O (**1**), [Co (HL)(OAc)].2H_2O (**2**), [Cu (HL)(Cl].4H_2O (**5**), and [Cu (HL)(OAc)].2H_2O (**6**) are similar, indicating that they are

TABLE 6 Thermal decomposition of the ligand (H_2L) and its metal chelates

No.	Chemical formula	TG range (°C)	DTG peak (°C)	Mass loss % Found	Mass loss % Calcd	Assignment
	$H_2L.0.5H_2O$ $C_{23}H_{22}N_5O_{2.5}S$	25–215	–	2.34	2.05	Loss of $0.5H_2O$
		215–390	285	32.03	32.50	Loss of $C_{10}H_7O$
		390–1000	485, 610	59.91	60.00	Loss of $C_{11}H_{14}N_5OS$
		At 1000		5.72	5.45	2 C[c]
1	[Co (HL)Cl].H_2O $C_{23}H_{22}N_5O_3SCoCl$	25–100	–	3.32	3.54	Loss of H_2O molecules[a]
		100–220	198	6.53	6.22	Loss of $0.5Cl_2$
		195–1000	266, 371	61.96	61.59	Loss of $C_{16.5}H_{20}N_5OS$
		At 1000		28.19	28.66	CoO + 6.5C[c]
2	[Co (HL)(OAc)].2H_2O $C_{25}H_{27}N_5O_6SCo$	25–100	39,80	6.16	6.48	Loss of $2H_2O$ molecules[a]
		100–220	202	10.11	10.26	Loss of CH_3COO
		220–1000	269, 375	60.64	60.21	Loss of $C_{18}H_{20}N_5OS$
		At 1000		23.09	23.05	CoO + 5C[c]
3	[Co(L)(H_2O)].H_2O.1.5EtOH $C_{26}H_{32}N_5O_{5.5}SCo$	25–180	145	17.71	17.65	Loss of $2H_2O$ + 1.5 EtOH[a]
		180–1000	256	69.67	69.85	Loss of $C_{23}H_{19}N_5OS$
		At 1000		12.62	12.50	CoO[c]
4	[Ni(L)(H_2O)].2EtOH $C_{27}H_{33}N_5O_7Sni$	25–200	143	18.41	18.22	Loss of H_2O + 2 EtOH[a]
		200–1000	270	69.45	69.10	Loss of $C_{23}H_{19}N_5OS$
		At 1000	–	12.14	12.68	Ni[c]
5	[Cu (HL)Cl].4H_2O $C_{23}H_{22}N_5O_7SCuCl$	25–150	98	11.98	11.55	Loss of $4H_2O$ molecules[a]
		150–250	177	5.89	5.13	Loss of $0.5Cl_2$
		250–1000	274	52.93	53.48	Loss of ($C_{15}H_{20}N_5O_2S$)
		At 1000		29.20	28.84	CuO + 8C[c]
6	[Cu (HL)(OAc)].2H_2O $C_{25}H_{27}N_5O_6SCu$	25–110	58	6.12	5.77	Loss of $2H_2O$ molecules[a]
		110–250	180(b)	10.02	10.34	Loss of CH_3COO[b]
		250–1000		54.56	54.52	Loss of $C_{15.25}H_{20}N_5OS$
		At 1000		29.30	29.37	CuO + 7.75C[c]

Note. DTG, Differential thermal gravity; TG, thermal gravity.
[a] Dehydration.
[b] Desolvation.
[c] Final residue.

isothermal. The theromgrams showed weight losses within 25–100°C due to the dehydration process. The compounds [Co (HL)Cl].H_2O (**1**) and [Co (HL)(OAc)].$2H_2O$ (**2**) started decomposition at 100°C, while the chelates [Cu (HL)(Cl].$4H_2O$ (**5**) and [Cu (HL)(OAc)].$2H_2O$ (**6**) begin to decompose at 110 and 150°C, respectively. The decomposition process was achieved mainly through two processes. The first step was TG weight losses corresponding to the removal of coordinated anions in the temperature range 100–220°C as shown in Table 6. The thermograms for these compounds revealed a varying weight loss within the range ~220–1000°C corresponding to organic ligand pyrolysis, leading to M(II) oxides with contamination with variable amounts of carbon atoms as a final product of the thermal decomposition process.

The thermoanalytical data and thermograms of the tetrahedral chelates [Co(L)(H_2O)].H_2O.1.5EtOH (**3**) and [Ni(L)(H_2O)].2EtOH (**4**) decompose in a similar way (Supporting Information Figure S7). The thermal degradation processes occurred via two distinct pyrolytic steps. The first steps are accompanied by weight losses of 17.71 and 18.41% within the range 25–200°C for **3** and **4**, respectively, consistent with the elimination of ethanol and coordinated water molecules in one step.[67] The second steps are characterized by sharp DTG peaks at $T_{\text{max.}}$ = 256 and 270°C and weight losses of 69.67% and 69.45% for **3** and **4**, respectively, due to complete ligand pyrolysis leaving CoO and NiO as final residue.

3.7 | Electron Spin Resonance (ESR) spectra of Cu(II) chelates

The X-band electron spin resonance spectra of the polycrystalline thiosemicarbazone Cu(II) chelates **5–7** were recorded at room temperature and the values of the spin Hamiltonian parameters of the chelates were calculated and are presented in Table 7.

The shape of the electron spin resonance spectra of the chelates is consistent with square planar geometry around each Cu(II) center in the chelates, which agrees with the electronic spectral data.

The electron spin resonance spectra of chelates **5–7** show two different types of geometrical species. Compounds **6** and **7** show a typical axial spectrum with well-defined parallel and perpendicular spin ($g_{//}$ and $g_{\perp}$) being assignable. Spectrum of the chelate **5** shows three resonance signals and the effective *g* values were found to be g_1 = 2.041, g_2 = 2.162, and g_3 = 2.214. The values of g_1 and g_2 for compound **5** are very close, indicating that the rhombic distortion is very small and the decreasing order of $g_3 > g_2 > g_1$ suggests the anisotropy of the chelate. The trend $g_{//} > g_{\perp} > 2.0023$ shown for all chelates (for *g* tensors with orthorhombic splitting we take $g_{\perp} = (g_1 + g_2)/2$[68]) shows that the unpaired electron most likely resides in the $d_{x^2-y^2}$ orbital, implying $^2B_{1g}$ as the ground state, which is characteristic of square planar geometry.[69,70] For chelates with $d_{x^2-y^2}$ ground state, strong interaction along the *z* axis is complemented by an increase in the value of $g_{//}$. Strong axial bonding causes an increase in the length of the bond in the *x–y* plane which leads to a decrease in both in-plane covalency and the energy of the $d_{x^2-y^2}$ transition. Both these effects tend to increase the value of $g_{//}$. Kivelson and Neiman have shown that $g_{//}$ is the most sensitive function for representing covalency.[71] For the ionic environment, the $g_{//}$ value is normally 2.3 or higher and less than 2.3 for the covalent character to the metal-ligand bonds in chelates. It is obvious from Table 7 that the $g_{//}$ obtained is less than 2.3, indicating the covalent character of the metal–ligand bond in the existing chelates. Massacesi *et al.* reported that $g_{//}$ is 2.3–2.4 for Cu–O bonds, 2.2–2.3 for Cu–N bonds and mixed Cu–N and Cu–O systems, and 2.1–2.2 for Cu–S bonds.[72] For the current chelates $g_{//}$ is 2.214–2.225, confirming the presence of Cu–O, Cu–N, and Cu–S bonds in these compounds. The parameter *R* ($R = (g_2 - g_1)/(g_3-g_2)$ for rhombic systems) calculated for the compound **5** is 0.70, i.e., $R < 1$, indicating a $d_{x^2-y^2}$ ground state for the Cu(II) ion.[73]

TABLE 7 Electron spin resonance spectral parameters of the Cu(II) chelates 5–7

Parameter	Chelate 5	Chelate 6	Chelate 7
$g_{//}/g_3$	2.214	2.219	2.225
g_2	2.162		
$g_{\perp}/g_1$	2.041	2.048	2.051
$g_{av}{}^a$	g_o = 2.139	2.105	2.109
G	2.123	4.742	4.551
$A_{//} \times 10^{-4}$ cm^{-1}	174		
$A\perp \times 10^{-4}$ cm^{-1}			
Δ_2	16129	15503	16393
Δ_3	21505	20833	21739
$k^2_{//}$	0.515	0.507	0.551
$k^2_{\perp}$	0.531	0.575	0.639
K	0.73	0.55	0.61
α^2	0.57		
β^2	0.90		
γ^2	0.93		
f	127		

[a] $g_{av} = (2\,g_{\perp} + g_{//})/3$, $K = (2K_{\perp} + K_{//})/3$.

The axial geometric parameter G, which is a measure of the exchange interaction between the Cu(II) centers in the polycrystalline solids, is calculated using $G = (g_{//} - 2.0023)/(g_{\perp} - 2.0023)$ for axial spectra and $G = (g_3 - 2.0023)/(g_{\perp} - 2.0023)$, where $g_{\perp} = (g_1 + g_2)/2$, for rhombic spectra. According to Hathaway and Billing,[68] if $G > 4$, the exchange interaction between Cu(II) centers in the solid state is negligible, but if $G < 4$ there is considerable exchange interaction in the solid state chelates. The calculated G values for the Cu(II) chelates are given in Table 7 and suggest that there is no exchange interaction in solid chelates except for chloro compound **5**.

The spectrum of chelate **5** (Supporting Information Figure S8), display a hyperfine anisotropy electron spin resonance spectrum with the defined hyperfine structure on the lower field region owing to the interaction between the unpaired electron of the Cu(II) ion with its nucleus, where the values of g and A are used to determine the empirical factor $f = g/A$, which is used as an index for tetragonal distortion.[74] A value of f in the range 105–135 cm indicates square planar geometry whereas larger values indicate tetragonally distorted chelates.[75] The f value of the investigated chelate ($f = 127$) indicates square planar geometry.

The bonding factors α^2, β^2, and γ^2, which can be used as a measure of the covalence of the in-plane σ bonds, and in-plane and out-of-plane π bonds, respectively, were calculated. α^2 was calculated by the following equation[71,76]:

$$\alpha^2 = A/0.036 + (g - 2.0023) + 3/7(g_{\perp} - 2.0023) + 0.04.$$

If the value of $\alpha^2 = 0.5$, this indicates a complete covalent character, while a value of $\alpha^2 = 1$ suggests complete ionic bonding. The calculated value of α^2 for the [Cu(HL)(ClO_4)]chelate is 0.54, representing a portion of unpaired electron density located on the Cu(II) ion.

The orbital reduction factors K and $K_{\perp}$ ($K^2 = \alpha^2\beta^2$ and $K^2{}_{\perp} = \alpha^2\gamma^2$), which are the parallel and perpendicular components of the orbital reduction factor and give significant information about the nature of the bonding in Cu(II) chelates, can be calculated using the following expressions[67]:

$$K^2 = (g - 2.0023)\Delta E_2/8\lambda_0$$

$$K^2{}_{\perp} = (g_{\perp} - 2.0023)\Delta E_3/2\lambda_0$$

where λ_o is the spin-orbit coupling constant of the free Cu(II) ion ($\lambda_0 = -828$ cm^{-1}) and $\Delta E_2 = {}^2B_{1g} \rightarrow {}^2A_{1g}$ and $\Delta E_3 = {}^2B_{1g} \rightarrow {}^2E_g$ may be used to measure the degree of covalency of the in-plane π bonding and out-of-plane π bonding, respectively. Hathaway[68] states that, for pure σ bonding $K \cong K_{\perp} \cong 0.77$ and for in-plane π bonding $K < K_{\perp}$, while for out-of-plane π bonding $K > K_{\perp}K_{\perp}$. For chelate **5**, $K < K_{\perp}$, indicating considerable in-plane π bonding.[77] Moreover, lower values of K than unity

TABLE 8 Electrochemical data for the ligand and its metal chelates

Compound	E_{pa}	E_{pc}	$E_{1/2}$	ΔE_p (mV)
H_2L	1.33	–	–	–
	1.55	–	–	–
[Co(HL)Cl].H_2O	0.66	–	–	–
	0.75	–	–	–
[Co(HL)(OAc)].2H_2O	1.32	1.18	1.250	140
	1.54	1.41	1.475	130
[Co(L)(H_2O)]. H_2O.1½EtOH	0.85	0.78	0.815	70
	1.19	–	–	–
	1.38	–	–	–
[Ni(L)(H_2O)].2EtOH	1.01	0.84	0.925	170
	1.31	–	–	–
	1.52	–	–	–
[Cu(HL)(Cl].4H_2O	1.05	–	–	–
	1.35	–	–	–
[Cu(HL)(OAc)].2H_2O	0.91	0.65	0.780	260
	1.28	–	–	--
[Cu(HL)(ClO_4].H_2O	0.62			

Note. $\Delta E_p = (E_{pa} - E_{pc})$ where E_{pa} and E_{pc} are anodic and cathodic potentials, respectively; $E_{1/2} = 0.5(E_{pa} + E_{pc})$; scan rate: 100 mV/s.

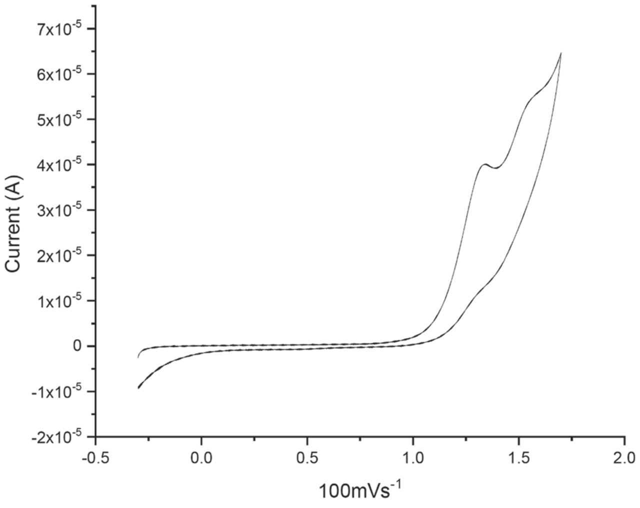

FIGURE 6 Cyclic voltammogram of the ligand H_2L at scan rate 100 mV/s

(0.55–0.75) are revealing of their covalent environment.[78] In addition, the values of β^2 and γ^2 (0.76 and 1.27, respectively) for metal chelate **5** reflect the presence of in-plane π bonding and ionic character of out-of-plane π bonding.[79]

3.8 | Electrochemical studies

The electrochemical properties of the synthesized ligand and its chelates were studied by cyclic voltammetry measurement in the range of 2.0 to −0.5 V. The voltammetric data are presented in Table 8 and the values shown are in agreement with the reported values for redox processes of similar ONS chelates.[79] The observed cyclic voltammograms are characterized by either irreversibility or quasi-reversibility as shown by wide separation of anodic and cathodic peaks, as well as the absence or marked reduction in the peak height of the reverse scan.

The voltammogram of the ligand (Figure 6) shows two irreversible anodic peaks at E_{pa} = 1.33 V and E_{pa} = 1.55 V, which were assigned to oxidations at the azomethine and thione groups of the thiosemicarbazone moiety.[80,81] The shift of redox peaks to a different potential in the spectra of the chelates indicates the coordination of the ligand with metal ions where most chelates under study show one quasi-reversible oxidation process as manifest by the peak-to-peak separation, $\Delta E_p > 100$ mV.[82]

For the Co(II) chelate **3**, there are three oxidation peaks on the voltammogram (Figure 7). The first peak at E_{pa} = 0.85 V, which is not shown by the corresponding ligand, is quasi-reversible ($E_{1/2}$ = 0.815 V) and specifies oxidation of Co(II) to Co(III). The positive potential specifies that the metal in the lower oxidation state is strongly bound to the ligand, which indicates that the metal center has an equal attitude towards donor atoms.[83]

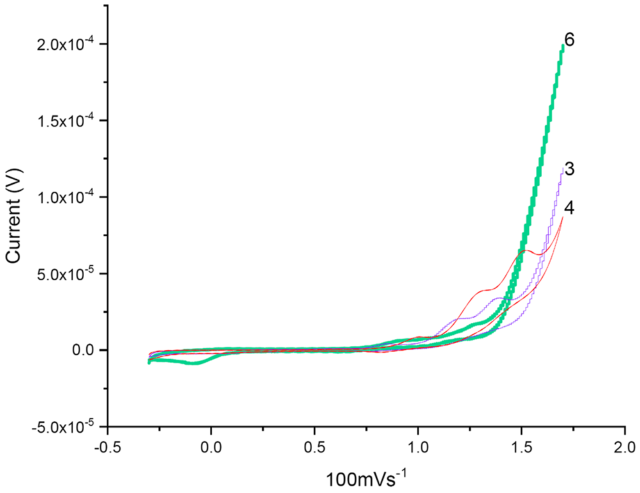

FIGURE 7 Cyclic voltammograms of complexes **3**, **4**, and **6**

Ni(II) chelate **4** shows two irreversible oxidation peaks at E_{pa} = 1.31 V and E_{pa} = 1.52 V corresponding to the ligand moiety (Figure 7). The chelate also exhibits one quasi-reversible redox wave, indicating that Ni(II) chelate undergoes Ni(II)/Ni(III) oxidation at E_{pa} = 1.01 V and corresponding reduction at E_{pc} = 0.84 V.[84]

Extensive studies were reported on four coordinate Cu(II) chelates.[79,85] Chelate **6** with a coordinated acetate ligand showed one quasi-reversible Cu (II)–Cu(III) redox couple at $E_{1/2}$ = 0.78 V with a peak-to-peak separation (ΔE_p) of 260 mV. Chelates **5** and **7** with coordinated chloro and perchlorate ligands only showed oxidation responses at E_{pa} = 1.05 V and E_{pa} = 0.62 V, respectively, which were attributed to irreversible electrochemical behavior (Figure 7).

Generally, the nature of the central metal atom weakly affects the values of the oxidation potentials of these chelates. However, in comparison with the free ligand HL, we note a sensitivity of the potential values of the oxidation of thiosemicarbazone groups to the coordination of the azomethine, thione/thiol, and phenolate fragments to the transition metal ion.

3.9 | Biological activity

The *in vitro* antibacterial activities of the thiosemicarbazone ligand and its metal chelates were assessed against the human pathogenic bacteria Gram-positive*S. aureus* and Gram-negative*E. coli* using the disc diffusion method. The radial growth of the colony was recorded on completion of the incubation, and the mean diameter for each compound at a concentration of 5 mg/ml was recorded. Dimethyl sulfoxide (DMSO) was used as a solvent and the mean inhibition zone was measured and compared with the standard antibiotic, enrofloxacin (5 mg/ml). The images of the zone of inhibition were shown in Diagram 1 and the results are presented in Table 9, taking into consideration the stability of the compounds over a range of pH (5–11) to fit their usefulness in antibacterial studies.

It can be seen that all the chelates are more effective bactericides than the ligand. The detected activities of the metal chelates are analogous with those conveyed for chelates prepared using thiosemicarbazones as ligands.[86] This improvement of the activity can be elucidated based on chelation theory.[87–91] Chelation decreases the polarity of the metal ion significantly, mostly owing to the partial sharing of its positive charge with donor groups and possible π-electron delocalization on the entire chelate ring. Chelation is not the single

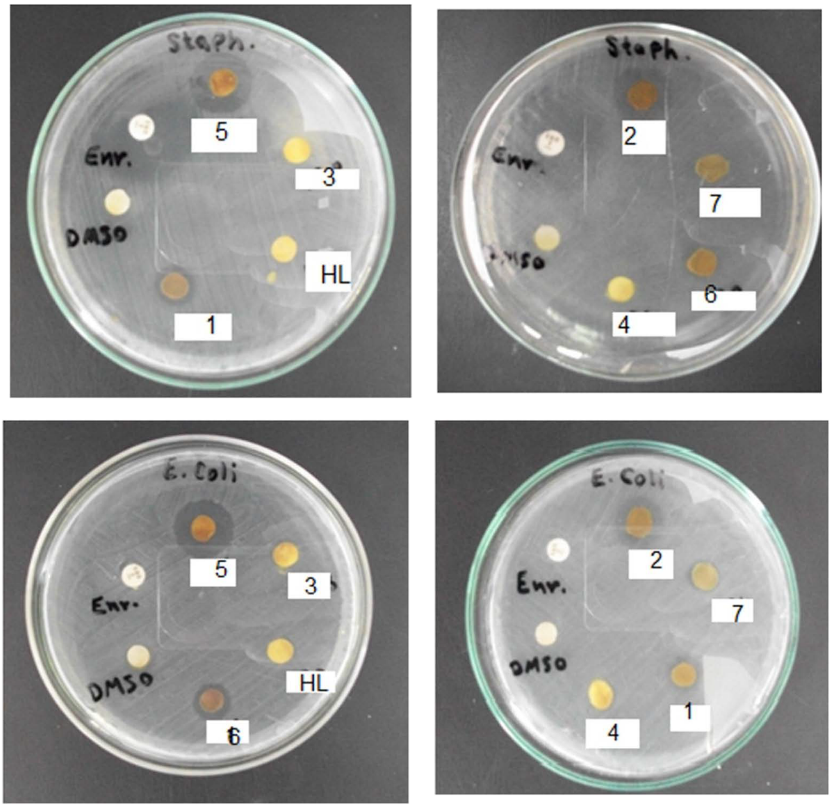

DIAGRAM 1 The zone effect of the ligand H_2L and its complexes

TABLE 9 *In vitro* antibacterial activity of tested thiosemicarbazone ligand and its metal chelates

	Microorganism inhibition zone diameter (mm)	
	Gram-positive bacteria	**Gram-negative bacteria**
Compounds	***Staphylococcus aureus***	***Escherichia coli***
HL	8.1	7.6
1	10.0	11.0
2	9.8	8.7
3	8.6	8.3
4	14.3	13.7
5	14.8	16.1
6	14.6	13.9
7	11.6	10.1
Dimethyl sulfoxide (DMSO)	–	–
Enrofloxacin	26.3	–

principle for antibacterial activity, where some vital factors such as the nature of the metal ion, the nature of the organic ligand, coordinating sites, the geometry of the chelate, concentration, hydrophilicity, lipophilicity, and occurrence of co-ligands have a significant effect. Steric and pharmacokinetic factors also have a significant role in determining the effectiveness of an antimicrobial agent. A way from this, the mode of action of these compounds may also invoke hydrogen bonding between the >C=N–N=CS– group and the active centers of biomolecules and therefore interfere with normal cell processes. A heterocyclic ligand with many donor atoms has a greater chance of interaction either with nucleoside bases or with the essential metal ions present in the biosystem, so it can be used as bactericides since they tend to interact with some enzymatic functional groups to achieve higher coordination numbers.[92,93] Furthermore, enhancement in antibacterial activity on coordination with a metal ionmay due to the existence of donor atoms in the ligand or the formed unsaturated coordinately species which inhibit enzyme production.[94] All metal chelates under study exhibited better activity than the thiosemicarbazone ligand (H_2L) against the tested strains of bacteria. Furthermore, the free ligand and its metal chelates were more active against Gram-positive bacteria (*S. aureus*) compared to Gram-negative bacteria (*E. coli*).[95] In Gram-positive bacteria, chelates **4**, **5**, and **6** were highly active with comparable zones of inhibition of 14.3, 14.8, and 14.6 mm, which is almost two times better than the ligand. However, in Gram-negative bacteria metal chelate **5** was the most active, screening a comparable zone of inhibition of 16.1 mm, displaying better efficiency than the ligand and the other chelates. It is worth note that the antibacterial activity of the compounds against particular kinds of bacteria (Table 8) showed that Cu(II) > Ni(II) > Co(II).[96] On comparing the antibacterial activity of the Schiff base ligand (8.1 and 7.6 mm) with 3,5-dichlorosalicylaldehyde-*N*^{4}-cyclohexylthiosemicarbazone (0 and 4 mm), it can be seen that the prepared ligand exhibits more forceful activity against *S. aureus* and *E. coli*, respectively.[97] Also, comparing the antibacterial activity of compound **6** (14.6 and 13.9 mm) with [Cu(dsct)(bipy)]·DMF (0 and 8 mm), we found that the compound **6** is more efficient against *S. aureus* and *E. coli*. On comparing the zone of inhibitions of $CuCl_2$ compound **5** (14.8 mm) with $[Cu(MnTSC)_2]$ (2.86 mm), the results show that *former* has better activity than the latter against the bacterial strain *S. aureus*.[98] In the same way we found that compound **4** has better activity (14.3 and 13.3 mm) than the Ni(II) compound $[NiCl(L^1)]$ (14.0 and 13.0) against *S. aureus* and *E. coli*, respectively.[99]

4 | CONCLUSION

In this study, Co(II), Ni(II), and Cu(II) chelates with a tridentate thiosemicarbazone ligand were synthesized and characterized by various analytical and spectroscopic techniques. Based on physicochemical studies the Co(II) and Ni(II) chelates adopted tetrahedral geometry while the Cu(II) chelates demonstrated square planar geometry as shown in Scheme 1. Furthermore, antimicrobial studies showed that the metal chelates have better inhibitory activity against the tested *S. aureus* and *E. coli* bacteria compared to the unchelated Schiff base thiosemicarbazone. The inhibitory effect can be correlated with the decrease in polarity of the metal ion, due to chelation, this could reinforce the lipoliphilicity of the metal chelates and thus favors its penetration through the lipid layer of the bacterial membranes. The results obtained are very interesting and promising, particularly when compared with the activity displayed by comparable compounds.

ACKNOWLEDGEMENTS

The authors thank Dr. El Hassane Anouar for helping in the computational part and for useful discussions.

ORCID

Ayman K. El-Sawaf https://orcid.org/0000-0002-0511-4061

REFERENCES

[1] V. A. Kumar, Y. Sarala, A. Siddikha, S. Vanitha, S. Babu, A. V. Reddy, *J. Appl. Pharmaceut. Sci.* **2018**, *8*, 71.

[2] E. Dilanyan, T. Ovsepyan, F. Arsenyan, B. Garibdzhanyan, *Pharm. Chem. J.* **1996**, *30*, 678.

[3] P. Kadaba, K. Pankaja, L. Zhaiwei, Hydrazones, hydrazines, semicarbazones, and thiosemicarbazones derived from pyridyl ketones as anticonvulsant drugs and excitatory amino acid antagonists. *US Patent* **1999**, *5*, 527.

[4] R. J. Anderson, I. S. Cloudsdale, R. J. Lamoreaux, K. Schaefer, J. Harr, Compositions containing semicarbazones, in, Google Patents, **1997**.

[5] S. Yamaguchi, K. Uesugi, *Nippon Kaisui Gakkaishi* **1995**, *49*, 352.

[6] C. S. Allardyce, A. Dorcier, C. Scolaro, P. J. Dyson, *Appl. Organomet. Chem.* **2005**, *19*, 1.

[7] A. D. Khalaji, E. Shahsavani, N. Feizi, M. Kučeráková, M. Dušek, R. Mazandarani, A. Amiri, *C. R. Chim.* **2017**, *20*, 125.

[8] M. Şahin, S. Eğlence-Bakır, M. Alpay, S. Alpay, R. Özmerdivenli, B. Ülküseven, *Inorg. Chim. Acta* **2020**, *502*, 119347.

[9] M. Muralisankar, S. Sujith, N. S. Bhuvanesh, A. Sreekanth, *Polyhedron* **2016**, *118*, 103.

[10] A. K. El-Sawaf, F. El-Essawy, A. A. Nassar, E.-S. A. El-Samanody, *J. Mol. Struct.* **2018**, *1157*, 381.

[11] E.-S. A. El-Samanody, A. K. El-Sawaf, M. Madkour, *Inorg. Chim. Acta* **2019**, *487*, 307.

[12] A. Vogel, J. Bassett, *Vogel's textbook of quantitative inorganic analysis, including elementary instrumental analysis*, 4th ed., Longman, London and New York **1978**.

[13] A. K. El-Sawaf, M. A. Azzam, A. M. Abdou, E. H. Anouar, *Inorg. Chim. Acta* **2018**, *483*, 116.

[14] A. D. Becke, *J. Chem. Phys.* **1993**, *98*, 5648.

[15] M. Andersson, P. Uvdal, *J. Phys. Chem. A.* **2005**, *109*, 2937.

[16] F. Furche, R. Ahlrichs, *J. Phys. Chem.* **2002**, *117*, 7433.

[17] G. Scalmani, M. J. Frisch, B. Mennucci, J. Tomasi, R. Cammi, V. Barone, *J. Phys. Chem.* **2006**, *124*, 094107.

[18] J. Gauss, *J. Chem. Phys.* **1993**, *99*, 3629.

[19] J. Tomasi, B. Mennucci, R. Cammi, *Chem. Rev.* **2005**, *105*, 2999.

[20] D. Jacquemin, V. Wathelet, E. A. Perpete, C. Adamo, *J. Chem. Theory Comput.* **2009**, *5*, 2420.

[21] M. J. Frisch, H. B. Schlegel, G. E. Scuseria, M. A. Robb, J. R. Cheeseman, G. Scalmani, V. Barone, B. Mennucci, G. A. Petersson, H. Nakatsuji, M. Caricato, X. Li, H. P. Hratchian, A. F. Izmaylov, J. Bloino, G. Zheng, J. L. Sonnenberg, M. Hada, M. Ehara, K. Toyota, R. Fukuda, J. Hasegawa, M. Ishida, T. Nakajima, Y. Honda, O. Kitao, H. Nakai, T. Vreven, J. A. Montgomery Jr., J. E. Peralta, F. Ogliaro, M. Bearpark, J. J. Heyd, E. Brothers, K. N. Kudin, V. N. Staroverov, R. Kobayashi, J. Normand, K. Raghavachari, J. C. Burant, S. S. Iyengar, J. Tomasi, M. Cossi, N. Rega, J. M. Millam, M. Klene, J. E. Knox, J. B. Cross, V. Bakken, C. Adamo, J. Jaramillo, R. Gomperts, R. E. Stratmann, O. Yazyev, A. J. Austin, R. Cammi, C. Pomelli, J. W. Ochterski, R. L. Martin, K. Morokuma, V. G. Zakrzewski, P. S. G. A. Voth, J. J. Dannenberg, S. Dapprich, A. D. Daniels, O. Farkas, J. B. Foresman, J. C. J. V. Ortiz, D. J. Fox, *Gaussian 09, Revision A.02*, Gaussian, Inc, Wallingford CT **2009**.

[22] A. Bauer, W. Kirby, J. C. Sherris, M. Turck, *Am. J. Clin. Pathol.* **1966**, *45*, 493.

[23] C. Sheikh, M. S. Hossain, M. S. Easmin, M. S. Islam, M. Rashid, *Biol. Pharm. Bull.* **2004**, *27*, 710.

[24] B. Prathima, Y. S. Rao, G. Ramesh, M. Jagadeesh, Y. Reddy, P. Chalapathi, A. V. Reddy, *Spectrochim. Acta, Part a* **2011**, *79*, 39.

[25] Y.-h. Li, B.-d. Wang, Z.-y. Yang, *Spectrochim. Acta, Part A* **2007**, *67*, 395.

[26] E.-S. A. El-Samanody, *Appl. Organomet. Chem.* **2018**, *32*, e4586.

[27] W. J. Geary, *Coord. Chem. Rev.* **1971**, *7*, 81.

[28] D. B. Lovejoy, D. R. Richardson, P. V. Bernhardt, *Acta Crystallogr., Sect. C: Cryst. Struct. Commun.* **2000**, *56*, 341.

[29] R. Prabhakaran, K. Palaniappan, R. Huang, M. Sieger, W. Kaim, P. Viswanathamurthi, F. Dallemer, K. Natarajan, *Inorg. Chim. Acta* **2011**, *376*, 317.

[30] E. M. Jouad, A. Riou, M. Allain, M. A. Khan, G. M. Bouet, *Polyhedron* **2001**, *20*, 67.

[31] S. Chandra, M. Pundir, *Spectrochim. Acta, Part A* **2007**, *68*, 883.

[32] S. Datta, M. G. Drew, S. Bhattacharya, *Indian J. Chem.* **2011**, *50*, 1403.

[33] M. Enamullah, M. A. Quddus, M. A. Halim, M. K. Islam, V. Vasylyeva, C. Janiak, *Inorg. Chim. Acta* **2015**, *427*, 103.

[34] M. Siwy, D. Sek, B. Kaczmarczyk, J. Wietrzyk, A. Nasulewicz, A. Opolski, *Anticancer Res.* **2007**, *27*, 1553.

[35] S. V. Amosova, N. A. Makhaeva, A. V. Martynov, V. A. Potapov, B. R. Steele, I. D. Kostas, *Synthesis* **2005**, *2005*, 1641.

[36] L. Larabi, Y. Harek, A. Reguig, M. Mostafa, *J. Serb. Chem. Soc.* **2003**, *68*, 85.

[37] S. Chandra, S. Bargujar, R. Nirwal, N. Yadav, *Spectrochim. Acta, Part A* **2013**, *106*, 91.

[38] I. Fleming, D. H. Williams, *Spectroscopic methods in organic chemistry*, McGraw-Hill, New York **1966**.

[39] M. Joseph, A. Sreekanth, V. Suni, M. P. Kurup, *Spectrochim. Acta, Part A* **2006**, *64*, 637.

[40] A. Iqbal, H. L. Siddiqui, C. Ashraf, M. Ahmad, G. W. Weaver, *Molecules* **2007**, *12*, 245.

[41] W. H. Mahmoud, M. Omar, Y. M. Ahmed, G. G. Mohamed, *Appl. Organomet. Chem.* **2020**, e5528.

[42] S. M. Emam, D. A. Tolan, A. M. El-Nahas, *Appl. Organomet. Chem.* **2020**, e5591.

[43] R. Prabhakaran, S. Renukadevi, R. Karvembu, R. Huang, J. Mautz, G. Huttner, R. Subashkumar, K. Natarajan, *Eur. J. Med. Chem.* **2008**, *43*, 268.

[44] G. Deacon, R. Phillips, *Coord. Chem. Rev.* **1980**, *33*, 227.

[45] M. Teotia, J. Gurtu, V. Rana, *J. Inorg. Nucl. Chem.* **1980**, *42*, 821.

[46] A. El-Dissouky, A. Fahmy, A. Amer, *Inorg. Chim. Acta* **1987**, *133*, 311.

[47] E.-S. A. El-Samanody, M. W. Polis, E. M. Emara, *J. Mol. Struct.* **2017**, *1144*, 300.

[48] M. Soriano-Garcia, J. Valdes-Martinez, R. Toscano, J. Gómez-Lara, *Acta Crystallogr., Sect. C: Cryst. Struct. Commun.* **1985**, *41*, 500.

[49] E. Gyepes, F. PavelcÏõÂk, *Collect. Czech. Chem. Commun.* *46*, 975.

[50] P. P. Netalkar, S. P. Netalkar, V. K. Revankar, *Polyhedron* **2015**, *100*, 215.

[51] D. X. West, M. M. Salberg, G. A. Bain, A. E. Liberta, *Transition Met. Chem.* **1997**, *22*, 180.

[52] A. B. P. Lever, *Inorganic electronic spectroscopy*, Elsevier, Amsterdam **1984**.

[53] N. Guskos, T. Dziembowska, G. Palios, S. Paraskevas, V. Likodimos, E. Grech, J. Typek, M. Wabia, E. Jagodzinska, *Pol. J. Chem.* **1995**, *69*, 1630.

[54] P. Gili, M. Palacios, M. Martin-Reyes, P. Martin-Zarza, C. Ruiz-Perez, F. Rodriguez-Romero, F. Lahoz, *Polyhedron* **1992**, *11*, 2171.

[55] L. Latheef, M. R. P. Kurup, *Spectrochim. Acta, Part a* **2008**, *70*, 86.

[56] B. Shaabani, A. A. Khandar, F. Mahmoudi, S. S. Balula, L. Cunha-Silva, *J. Mol. Struct.* **2013**, *1045*, 55.

[57] A. Q. Ali, S. G. Teoh, N. E. Eltayeb, M. B. K. Ahamed, A. A. Majid, *J. Coord. Chem.* **2014**, *67*, 3380.

[58] M. Mikuriya, H. Okawa, S. Kida, *Bull. Chem. Soc. Jpn.* **1980**, *53*, 3717.

[59] G. Gritzner, J. Kuta, *Pure Appl. Chem.* **1984**, *56*, 461.

[60] N. El-wakiel, M. El-Keiy, M. Gaber, *Spectrochim. Acta, Part A* **2015**, *147*, 117.

[61] O. M. Adly, *Spectrochim. Acta, Part A* **2011**, *79*, 1295.

[62] H. El-Ghamry, N. El-Wakiel, A. Khamis, *Appl. Organomet. Chem.* **2018**, *32*, e4583.

[63] C. Jorgensen, *Acta Chem. Scand.* **1962**, *16*, 2017.

[64] R. L. Dutta, A. Syamal, *Elements of Magneto Chemistry*, Affiliated East West Press, New Delhi **1993**.

[65] N. Sarı, S. Ç. Şahin, H. Öğütcü, Y. Dede, S. Yalcin, A. Altundaş, K. Doğanay, *Spectrochim. Acta, Part A* **2013**, *106*, 60.

[66] A. Sreekanth, M. R. P. Kurup, *Polyhedron* **2003**, *22*, 3321.

[67] E. S. A. El-Samanody, S. A. AbouEl-Enein, E. M. Emara, *Appl. Organomet. Chem.* **2018**, *32*, e4262.

[68] B. Hathaway, D. Billing, *Coord. Chem. Rev.* **1970**, *5*, 143.

[69] K. B. Gudasi, S. A. Patil, R. S. Vadavi, R. V. Shenoy, M. Nethaji, *Transition Met. Chem.* **2006**, *31*, 586.

[70] K. M. Raj, B. Vivekanand, G. Nagesh, B. Mruthyunjayaswamy, *J. Mol. Struct.* **2014**, *1059*, 280.

[71] D. Kivelson, R. Neiman, *J. Chem. Phys.* **1961**, *35*, 149.

[72] M. Massacesi, G. Ponticelli, V. B. Addepali, V. Krishnan, *J. Mol. Struct.* **1978**, *48*, 55.

[73] S. S. Kandil, A. El-Dissouky, G. Y. Ali, *J. Coord. Chem.* **2004**, *57*, 105.

[74] S. M. Romanowski, F. Tormena, V. A. Santos, M. D. Hermann, A. S. Mangrich, *J. Braz. Chem. Soc.* **2004**, *15*, 897.

[75] U. Sakaguchi, A. W. Addison, *J. Chem. Soc., Dalton Trans.* **1979**, 600.

[76] A. Maki, B. McGarvey, *J. Chem. Phys.* **1958**, *29*, 35.

[77] W. H. Mahmoud, G. G. Mohamed, M. M. El-Dessouky, *Spectrochim. Acta, Part A* **2014**, *122*, 598.

[78] H. A. El-Boraey, O. A. El-Gammal, *Spectrochim. Acta, Part A* **2015**, *138*, 553.

[79] R. P. John, A. Sreekanth, V. Rajakannan, T. Ajith, M. P. Kurup, *Polyhedron* **2004**, *23*, 2549.

[80] İ. Şener, Ç. Şahin, S. Demir, N. Şener, M. Gür, *J. Mol. Struct.* **2020**, *1203*, 127475.

[81] N. Arefyeva, A. Sandleben, A. Krest, U. Baumann, M. Schäfer, M. Kempf, A. Klein, *Inorganics* **2018**, *6*, 51.

[82] S. Chandra, R. Kumar, R. Singh, A. K. Jain, *Spectrochim. Acta, Part A* **2006**, *65*, 852.
[83] S. V. Baryshnikova, A. I. Poddel'sky, A. V. Cherkasov, I. V. Smolyaninov, *Inorg. Chim. Acta* **2019**, *495*, 118963.
[84] S. Kundu, A. K. Pramanik, A. S. Mondal, T. K. Mondal, *J. Mol. Struct.* **2016**, *1116*, 1.
[85] N. Raman, A. Kulandaisamy, C. Thangaraja, K. Jeyasubramanian, *Transition Met. Chem.* **2003**, *28*, 29.
[86] Z. H. Chohan, H. Pervez, A. Rauf, K. M. Khan, C. T. Supuran, *J. Enzyme Inhib. Med. Chem.* **2004**, *19*, 417.
[87] A. M. Abu-Dief, L. A. Nassr, *J. Iran. Chem. Soc.* **2015**, *12*, 943.
[88] A. M. Abu-Dief, L. H. Abdel-Rahman, A. A. Abdelhamid, A. A. Marzouk, M. R. Shehata, M. A. Bakheet, O. A. Almaghrabi, A. Nafady, *Spectrochim. Acta, Part A* **2020**, *228*, 117700.
[89] L. H. A. Rahman, A. M. Abu-Dief, R. M. El-Khatib, S. M. Abdel-Fatah, *Int. J. Nano. Chem* **2018**, *4*, 1.
[90] L. H. Abdel-Rahman, A. M. Abu-Dief, M. O. Aboelez, A. A. H. Abdel-Mawgoud, *J. Photochem. Photobiol., B* **2017**, *170*, 271.
[91] L. H. Abdel-Rahman, A. M. Abu-Dief, M. Rafat, *J. Bioorg. Chem* **2016**, *69*, 140.
[92] W. Levingson, P. Mikeleus, J. Jackson, W. Kaska, G. Schranzer, *Inorganic and Nutritional Aspects of Cancer*, Plenum Press, New York **1978**.
[93] Z. H. Chohan, Mahmood-ul-Hassan, K. M. Khan, C. T. Supuran, *J. Enzyme Inhib. Med. Chem.* **2005**, *20*, 183.
[94] Z. H. Chohan, M. Farooq, A. Scozzafava, C. T. Supuran, *J. Enzyme Inhib. Med. Chem.* **2002**, *17*, 1.
[95] A. S. Pires, J. Batista, D. Murtinho, C. Nogueira, A. Karamysheva, M. Luísa Ramos, B. F. Milne, N. T. Tavares, J. Gonçalves, A. C. Gonçalves, *Appl. Organomet. Chem.* **2020**, e5569.
[96] M. C. Rodríguez-Argüelles, A. Sánchez, M. B. Ferrari, G. G. Fava, C. Pelizzi, G. Pelosi, R. Albertini, P. Lunghi, S. Pinelli, *J. Inorg. Biochem.* **1999**, *73*, 7.
[97] N. A. Mathews, P. S. Begum, M. P. Kurup, *Appl. Organomet. Chem.* **2020**, *34*, e5294.
[98] F. A. Beckford, K. R. Webb, *Spectrochim. Acta, Part a* **2017**, *183*, 158.
[99] A. B. Ibrahim, M. K. Farh, P. Mayer, *Appl. Organomet. Chem.* **2019**, *33*, e4883.

SUPPORTING INFORMATION

Additional supporting information may be found online in the Supporting Information section at the end of this article.

How to cite this article: El-Sawaf AK, Abdel-Monem YK, Azzam MA. Synthesis, spectroscopic, electrochemical characterization, density functional theory (DFT), time dependent density functional theory (TD-DFT), and antibacterial studies of some Co(II), Ni(II), and Cu(II) chelates of (*E*)-4-(1,5-dimethyl-3-oxo-2-phenyl-2,3-dihydro-1*H*-pyrazol-4-yl)-1-(3-hydroxynaphthalen-2-yl) methylene) thiosemicarbazide Schiff base ligand. *Appl Organomet Chem*. 2020;e5729. https://doi.org/10.1002/aoc.5729